Towards a Multiscale, High-Resolution Model of the Human Brain

Katrin Amunts[1,2(✉)], Oliver Bücker[3], and Markus Axer[1]

[1] Research Centre Juelich, Institute of Neuroscience and Medicine (INM-1), Juelich, Germany
{k.amunts,m.axer}@fz-juelich.de
[2] Cecile and Oskar Vogt Institute for Brain Research, Heinrich Heine University Düsseldorf, Düsseldorf, Germany
katrin.amunts@uni-duesseldorf.de
[3] Juelich Supercomputing Centre (JSC), Research Centre Juelich, Juelich, Germany
o.buecker@fz-juelich.de

Abstract. To understand the microscopical organization including cellular and fiber architecture it is a necessary prerequisite to build models of the human brain on a sound biological basis. We have recently pushed the limits of current technology by creating the first ultra-high resolution 3D-model of the human brain at nearly cellular resolution of 20 microns, the BigBrain model. At the same time, 3D Polarized Light Imaging provides a window to analyze the fiber architecture, i.e., the way, how brain regions are inter-connected, with unprecedented spatial resolution at the micrometer level. Considering the complexity and the pure size of the human brain with its nearly 86 billion nerve cells, both approaches are most challenging with respect to data handling and analysis in the TeraByte to PetaByte range, and require supercomputers. Parallelization and automation of image processing steps open up new perspectives to speed up the generation of new, ultra-high resolution models of the human brain, to provide new insights into the three-dimensional micro architecture of the human brain.

Keywords: Ultra-high resolution brain models · BigBrain · Cytoarchitecture · Microstructure · Fiber architecture · UNICORE · Workflows

1 Introduction

The cerebral cortex of the human brain is a highly heterogeneous structure. Since the beginning of the 20th century it is well known that the cortex consists of organ-like units, which Brodmann and others have called cortical areas [1]. Using a light microscope, Brodmann observed that every cortical area showed a characteristic cytoarchitecture. Cytoarchitectonic features include the distribution of neurons, the presence of particular cell types such as giant Betz cells, which are characteristic for the primary motor area 4 [2–4], clustering of cell bodies, and the formation of cortical layers (thickness, density, etc.), which run in parallel to the cortical surface (Fig. 1). Based on such differences, Brodmann published his famous monograph and a map, which displayed 43 cytoarchitectonic areas. Most of the areas of the cerebral cortex

L. Grandinetti et al. (Eds.): BrainComp 2013, LNCS 8603, pp. 3–14, 2014.
DOI: 10.1007/978-3-319-12084-3_1

show 6 layers (isocortex or neocortex, because it is developed late during brain evolution) with the notable exception of the motor cortex, which looses its fourth layer during postnatal development [1, 5]. The different regions of the isocortex subserve sensory (e.g., visual, auditory, somatosensory, gustatory, vestibular, pain), motor, and multimodal associative (e.g., working memory, attention, goal-directed behaviour) functions. Non-isocortical regions have more (e.g., entorhinal cortex) or less (e.g., hippocampus) layers than the isocortex. Therefore, these regions are called allocortex. It is known, that this laminar pattern is related to the connectivity of neurons, and reflects the prevailing inputs and outputs of the layers. For example, Layer I contains many axons, which establish short and long-range intracortical connections. Layers II and III have ipsilateral and commissural connections with cortical areas in the same and the other hemisphere. Layer IV is the major target of the ascending thalamo-cortical input, whereas the neurons of layers V and VI project to subcortical targets (e.g., basal ganglia, thalamus, brain stem and spinal cord). It is estimated that each neuron of the cerebral cortex has approximately 7.000 synapses [6], i.e., contacts to other neurons; the precise number of synapses differs between layers [7].

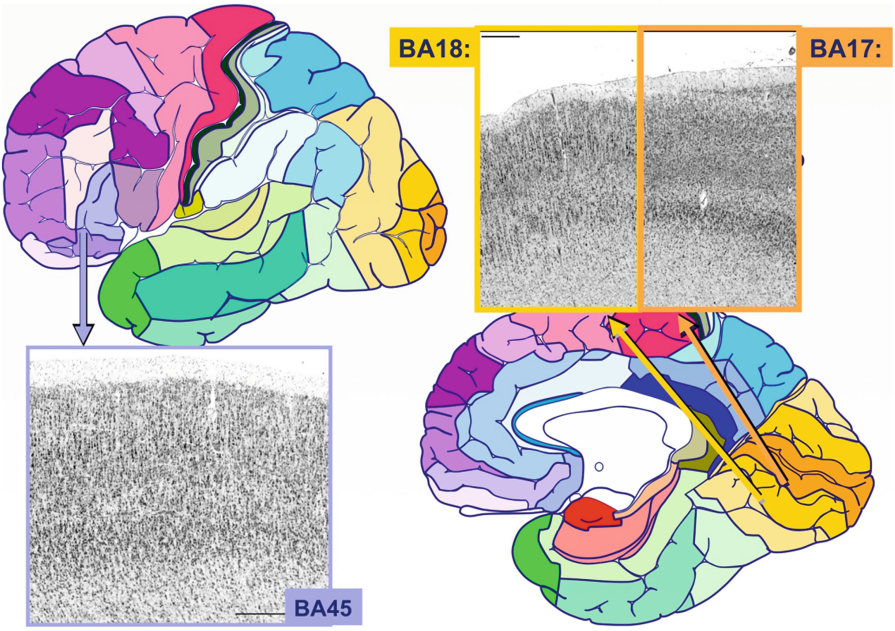

Fig. 1. Cytoarchitecture of the human cerebral cortex as basis of Brodmann's map from 1909. Each area of the cerebral cortex in Brodmann's map is labeled by a different color. The cytoarchitecture is illustrated in three cortical areas, BA 45, 17 and 18, belonging to different functional systems. Cell bodies are stained in black, and show a different distribution and density from the surface of the brain (top) to the cortex/white matter border. The space between the cell bodies is called neuropil. It contains synapses, dendrites and axons as major structures, which are relevant for connectivity between brain regions (Color figure online).

Using image analysis in combination with statistical tools of analysis, we have developed an approach to map cytoarchitectonic areas of the cerebral cortex in samples of (ten) human postmortem brains [8], and to register these maps in standard references space. Therefore, we have created probabilistic cytoarchitectonic maps in 3D. These maps can then be used, for example, as microstructural references for functional imaging studies of the living human brain. To allow comparisons between in vivo MR findings and postmortem cytoarchitectonic maps, the cytoarchitectonic maps have been made available in different software packages such as SPM toolbox (http://www.fz-juelich.de/inm/inm-1/DE/Forschung/_docs/SPMAnatomyToolbox/SPMAnatomyToolbox_node.html; [9–11]) and FSL (http://fsl.fmrib.ox.ac.uk/fsl/fslwiki/Atlases?highlight=%28probabilistic%29|%28maps%29). Or, they can be directly downloaded from the JuBrain website (https://www.jubrain.fz-juelich.de/apps/cytoviewer/cytoviewer-main.php).

The analysis of in vivo imaging studies based on cytoarchitectonic maps contributes to our knowledge of the relationship of the microstructural segregation of the human brain and the involvement of cortical areas and subcortical nuclei into a certain mental process (e.g., [12–14]), or they can be used as an atlas to guide or to interpret studies on connectivity and functional segregation as obtained during in vivo neuroimaging studies [15, 16]. The spatial resolution, which is necessary to address this type of structure-functional relationships is determined by the resolution of in vivo neuroimaging studies, which is in the range of 1 millimetre, i.e., at the mesoscopic level.

The highly complex organization of the human cerebral cortex at the level of single cells and their connections can be achieved only with a resolution at a few micrometres. It requires postmortem methods for the analysis, in most cases. As compared to investigations of the brains of non-human primates and rodents, the human brain is highly challenging due to the pure size of the whole human brain and the number of nerve cells (nearly 86 billion) in combination with the same number of glial cells [17, 18]. Neurons have a size of a several micrometers; the largest of them, the giant Betz cells of the primary motor cortex, can reach a height of 120 μm [19]. To address the microscopical organization of the human brain is not only challenging from the neuroscientific perspective, but also with respect to computational demands.

We have recently pushed the limits of existing three-dimensional brain data sets to a microscopical scale, and developed the BigBrain model [20]. The model is based on 7404 cell-body stained histological sections, which were corrected for artifacts, and reconstructed as a volume with 20-micrometre spatial resolution isotropic. This model provides a basis for extracting morphometric parameters characterizing the cortical folding, cell densities or cortical thickness, which can be used, e.g., for modelling and simulation. Moreover, it will serve as a new reference brain at a microscopical level, where structural and activity data from other researchers can be integrated while keeping the functionally relevant topography of the brain at the level of cortical layers and below [21]. In order to generate this model, methods of high performance computing were necessary – the total size of the data set was 1 TByte, and for the automated repair, 2D- and 3D alignment, and intensity correction 295,000 h were necessary for 100 iterations, measured on an AMD Opteron 2.1 GHz system. I/O operations hereby required a significant amount of time [20].

The architecture of cells in different brain areas and nuclei represents an important aspect of brain organization. It reflects differences in brain connectivity between brain

areas, and cortical layers. E.g. thalamic projections from the lateral geniculate body terminate in layer IVB of the primary visual cortex, whereas layer III pyramidal cells project to other cortical areas including those in the contralateral hemisphere [22], and layer V Meynert cells of the primary visual cortex form T-shape projections to higher associative visual areas [23]. The fiber architecture is functionally highly relevant, because the connectivity within a cortical area and between brain regions determines, to a high degree, the role that an area has in a certain network.

Diffusion imaging has been successfully used in visualizing the course of fiber tracts based on mathematical models. It takes advantage of the fact, that the diffusion of water molecules along nerve fibres is different from that across fibres [24–29]. Due to short acquisition times, diffusion imaging becomes more and more applied in order to analyse the connectome of healthy human subjects and patients [30–33]. Single axons and fibre bundles with a diameter of a few micrometres cannot be detected by diffusion imaging because of limitations in the spatial resolution.

Other techniques for analysing nerve fibres include macroscopical dissection techniques, myelin staining in histological sections and sensitive optical coherence tomography (PS-OCT) [34, 35], while tracing techniques, which are highly successful in determining the projections at the axonal level in brains of experimental animals (e.g., [23, 36, 37]), and which provide the "gold standard" are largely excluded for approaching human brain connectivity with a few exceptions [38]. As a consequence, human brain connectivity is less well analyzed than that of non-human primates, other mammals and invertebrates, although a profound understanding of connectivity would not only be crucial to approach human brain organization in the healthy brain, but also in a clinical context, to develop better diagnosis and therapies.

2 3D Polarized Light Imaging (3D-PLI) as a New Tool to Analyze Human Brain Fiber Architecture

3D-PLI is a neuroimaging technique that has opened up new avenues to study the complex nerve fiber architecture across the entire human brain at the micrometer level [39, 40]. Whole brain analysis in combination with high spatial resolution is a prerequisite to demonstrate both long-range fiber pathways and termination fields of single fibers emanating from the cortical layers. The method is based on unstained histological sections of postmortem brains, their analysis using a polarimeter, the calculation of fiber directions based on mathematical models, and the 3D-reconstruction of the data. In short:

Brain Preparation. The technique is applicable to unstained 60–100 micron thick histological sections of postmortem human brains generated with a cryostat microtome. The brain tissue is being fixed in 4 % of buffered formalin for at least three months before it undergoes the sectioning process. Depending on the section thickness and the sectioning plane (coronal, sagittal, or horizontal), about 1,500–3,000 sections are prepared per brain. These sections need to be imaged and analyzed in a complex workflow.

Basic Principles. It is the optical anisotropy of brain tissue that gives rise to pass polarized light through the unstained brain sections (i) to render microstructural details

within the sample and (ii) to derive their spatial orientations. The anisotropy is mainly caused by the nerve fibers, i.e. the long projections of neurons. Each fiber has distinct optical axes and interacts with light in a manner that is dependent on its three-dimensional orientation with respect to the incident light. This physical effect widely known as birefringence has been shown to be strongest for myelinated fibers [41]. This is mainly due to the radially arranged lipid bilayers largely consolidating the myelin sheath. Non-myelinated axons, however, also exhibit birefringence though with a much smaller detectable effect. In this case the macromolecular arrays of large molecules (i.e. neurofilaments) in the axon are likely to cause the birefringence.

Image Acquisition. In 3D-PLI, circularly polarized light is passed through the brain section and the local changes in the polarization state of light are measured using a dedicated polarimetric setup. Hence, the setup is equipped with a circular polarizer unit, a rotating linear polarizer and a specimen stage sandwiched in-between. Since these elements are built in a microscopic device with a Köhler illumination, each brain section can be scanned with a resolution at the level of nerve fiber diameters, thus, providing images with pixel sizes of $1.3 \times 1.3\ \mu m^2$. Due to the restricted field of view of this polarizing microscope ($2.7 \times 2.7\ mm^2$), to image an entire brain section, it is digitized tile-wise with overlapping contents. This leads to about 3,500 images or 140,000 × 100,000 pixels, respectively, for one coronal human brain section covering an area of $14 \times 10\ cm^2$. A typical 3D-PLI measurement includes eighteen complete scans per section rather than one, during the linear polarizer rotates between 0° and 170° around the stationary section. The acquired raw data set of the coronal section described above, therefore, requires 500 GB of storage space in total.

Core Image Analysis. Based on the eighteen measurements, a sinusoidal variation of the measured light intensity, referred to as light intensity profile, can usually be observed for each image pixel. The individual course of a light intensity profile essentially depends on the locally prevailing 3D fiber orientation. Deviations from the sinusoidal shape might indicate crossing fiber constellations, fibers pointing straight out of the sectioning plane, or simply no detectable birefringence. Basic principles of optics (Snell's law and Huygens-Fresnel principle) and the Jones calculus [42] mathematically link the measured light intensity profile to the fiber orientation described by a pair of angles (φ, α) or, alternatively, by a unit vector. The phase of the light intensity profile defines the in-section direction angle φ and its amplitude reflects the out-of-section inclination angle α. The image of all derived fiber orientations covering an entire brain section represents the fiber orientation map (FOM). An example of a FOM derived from 3D-PLI applied to a coronal section through the medial human brain is shown in Fig. 2.

Workflow. Collection and storage of the vast amount of data obtained with high-resolution 3D-PLI are not the only challenges we have to face. The core image analysis as described above is complemented by (i) image pre-processing approaches for artifact and noise removal (by means of image calibration and independent component analysis [43]) and by image post-processing approaches finally enabling the reconstruction of the entire series of sections into a coherent virtual fiber model of the human brain (e.g., segmentation of tissue and background, stitching of the tiles, non-linear image

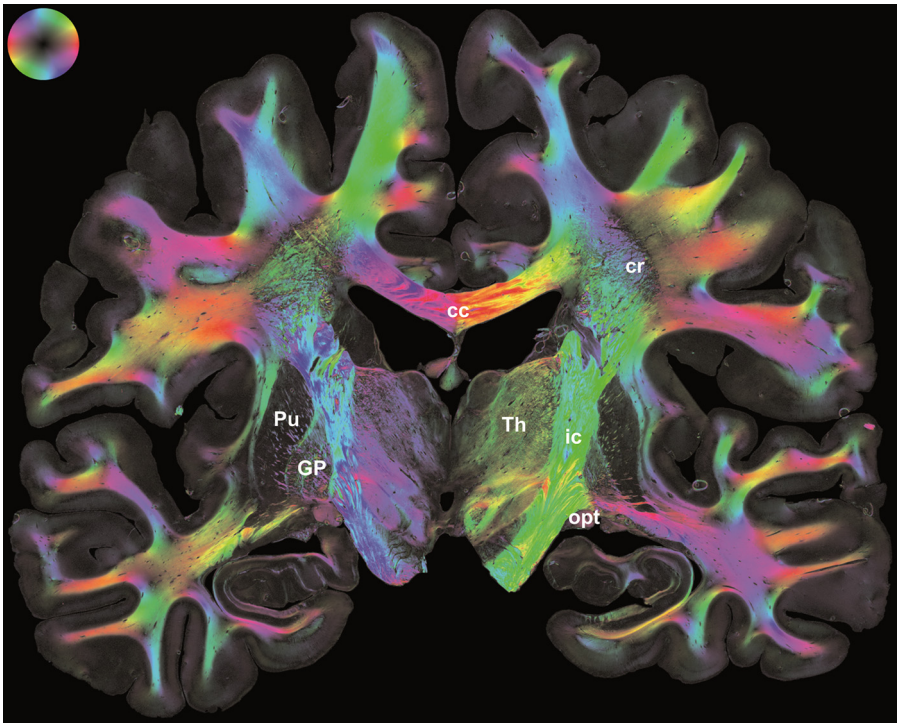

Fig. 2. Fiber orientation map of a coronal human brain section. Fiber orientations are encoded in HSV color space as indicated by the color sphere on the top left. The color encodes the direction angle φ and the saturation defines the inclination angle α (from saturated color for α = 0° to black for α = 90°). To give an example, transversal in-plane fibers are colored in red. Legend: cc = corpus callosum, cr = corona radiata, ic = capsula interna, Th = thalamus, Pu = putamen, GP = globus pallidus, opt = optic tract (Color figure online).

registration [44], fiber tractography [40]). Each of these steps is computationally intensive and needs to be compiled into an efficient and applicable workflow.

3 Automation and Parallelization of the 3D PLI Workflow

A first approach towards a fully automated and parallelized 3D-PLI workflow is being set up to utilize advanced supercomputing infrastructures efficiently. The main goal is to combine fast data access, complex (partially already developed) data analyses and high-performance computing in an easy-to-use manner, thus, cumulating in an automated workflow.

Supercomputing Environment. The Jülich Supercomputing Centre provides resources of the supercomputer JuDGE (Juelich Dedicated GPU Environment) for neuroscientific research. JuDGE is an IBM iDataPlex Cluster with 206 compute nodes. Each compute node has 2 Intel Xeon X5650 (Westmere) 6-core 2.66 GHz processors,

2 NVIDIA Tesla M2050 or M2070 (Fermi) GPUs and 96 GB main memory. This leads to a complete system of 2472 cores, 412 graphic processors, 19.8 TB main memory and 239 Teraflops peak performance [45]. In addition, access to the JuRoPA (Jülich Research on Petaflop Architectures) system is granted. This system has 3288 compute nodes each with 2 Intel Xeon X5570 (Nehalem-EP) 2.93 GHz quad-core processors and 24 GB main memory. This leads to complete system of 26304 cores, 79 TB main memory and a peak performance of 308 Teraflops. The system has a Linpack performance of 274.8 Teraflops and is placed since June 2009 in the Top500 list (actual: rank 136 [Nov 2013]) [46].

Platform. To assemble and streamline the 3D-PLI workflow, the UNICORE platform (Uniform Interface to Computing Resources) is used. This framework offers a ready-to-run grid system including client and server software. UNICORE enables distributed computing and makes data resources available in a seamless and secure way in intranets and the internet. [47] The implementation of UNICORE entails benefit for developers as well as for users. In the stage of developing a new software package for the workflow, for example, careful parameter optimization has to be performed. A structured call of the software with an iterating set of parameters can be managed easily with UNICORE.

Furthermore, even an untrained neuroscientist can do complex data analysis and routine data production without knowing all details about the different inputs, calls and requirements of individual software packages of the workflow. The number of variables to be declared by the user can be reduced to a minimum and the conversion of the raw data set into a FOM is done automatically. This clearly minimizes operation failures as compared to manual calls of individual software packages.

Optimized Workflow. In general, the parallelization is being realized at the level of the implemented algorithms, the processing strategies, and the workflow itself. While the individual parallelization of the algorithms is a developer specific task, the latter two types of parallelization can be done by UNICORE without having deep knowledge in using supercomputers.

Individual applications such as image segmentation and stitching as well as the determination of the fiber orientations are optimized in terms of internal usage of CPUs or GPUs or a hybrid usage of both units. In addition, some of the applications enable to process images or even image pixels independently from each other and can, therefore, be treated in parallel. The calibration procedure is an adequate candidate to be applied pixel-wise by farming. Applications in the workflow that are independent from each other are performed in parallel. This is the case for the image segmentation and image stitching, for example. In order to take advantage of specific features of different supercomputers (e.g., GPU vs. faster CPU), both systems JuDGE and JuRoPA are addressed within the workflow. It turns out to be an asset to utilize the faster CPUs of the JuRoPA system for the stitching application and the core image analysis. It is important to take into account that a better speedup can be used up by the data transfer between the systems. In our constellation it is possible to copy the data from the GPFS file system of JuDGE to the Lustre Storage of JuRoPA instead of transferring the data by uftp [48]. A schematic of the optimized workflow is shown in Fig. 3.

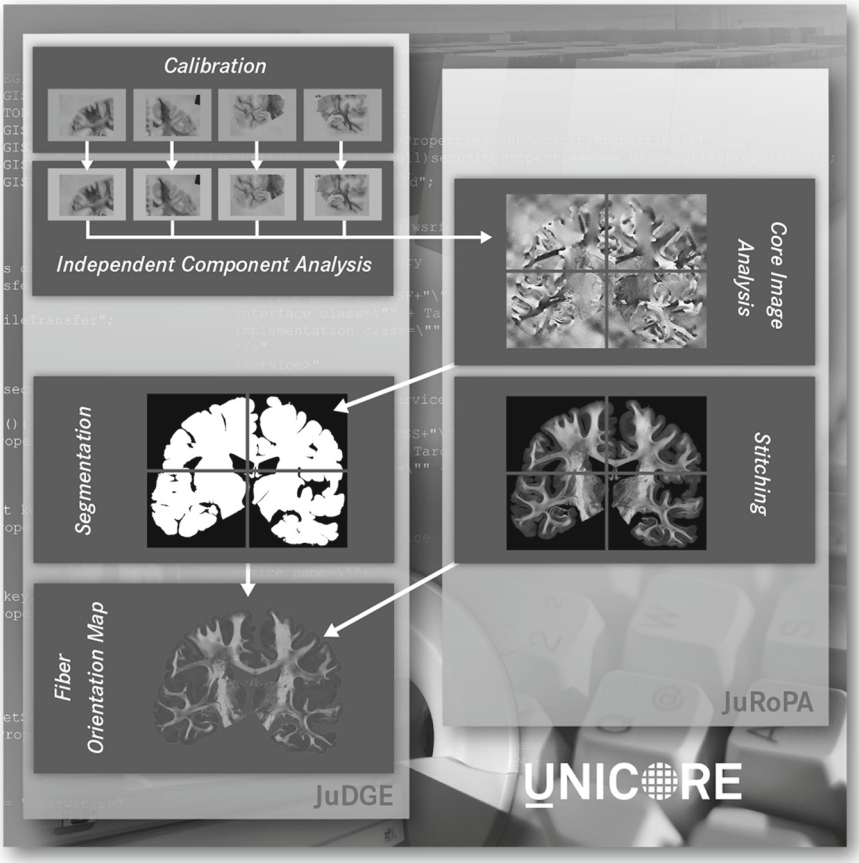

Fig. 3. Optimized workflow for 3D-PLI. UNICORE builds the framework to manage software package calls with input parameters and to organize the distributed calculation using JuDGE or JuRoPA.

The optimized 3D-PLI workflow for an individual high-resolution brain section can be reduced to a few hours as compared to several days or even weeks. As a consequence from the gained speedup, images with sizes far above 4 GB can now be processed at reasonable time scales, however, at the expense of the used data format. The file format NIfTI format (Neuroimaging Informatics Technology Initiative) [49], commonly used in neuroscience has to be exchanged by a container format, which is able to handle images substantially larger than 4 GB. Since this amount of data cannot be handled in a useful manner with sequential IO, parallel HDF5 [50] is the format of choice. Clearly, only the described workflow approach with the appropriate file format will allow an effective and fast processing of thousands of brain sections with 3D-PLI in the near future.

4 Conclusions

In future, we have to face several PetaBytes of data originating from postmortem studies (including 3D-PLI) to be collected, archived, analyzed, and finally integrated into a joint virtual model of the human brain. Specific challenges are posed by the multi-modal and multi-scale features of the obtained structural data, which characterize individual voxels in individual brains at different levels of detail and abstraction. Scalars, vectors or even more advanced mathematical objects are typically used to describe brain characteristics at the nanometer scale up to the millimeter scale. Comparison and visualization of such data, therefore, require common data access, and standardized scientific data formats and reference systems.

For 3D-PLI we have started to set up a customized e-infrastructure to parallelize and automatize the complex workflow, which was demonstrated to be beneficial in many aspects. The user can initiate a workflow calculation without knowing all tools and supercomputers used in the entire process, for example. Clearly, the computation time is speeded up significantly while the reproducibility of results is much better.

Acknowledgement. The authors thank Janine Klapper for help in preparing the manuscript, and Thomas Lippert for scientific discussion and support. Daniel Mallmann and André Giesler from the "Federated Systems and Data" group at the Jülich Supercomputing Centre generously assisted with the adaptation of UNICORE to the specific workflow requirements.

References

1. Brodmann, K.: Vergleichende Lokalisationslehre der Großhirnrinde in ihren Prinzipien dargestellt auf Grund des Zellenbaues. Barth JA, Leipzig (1909)
2. Brodmann, K.: Beiträge zur histologischen Lokalisation der Grosshirnrinde. I: Die Regio Rolandica. Beiträge zur Lokalisation der Grosshirnrinde II, 79–107 (1903)
3. Sherwood, C.C., Lee, P.W.H., Rivara, C.B., Holloway, R.L., Gilissen, E.P.E., Simmons, R. M.T., Hakeem, A., Allman, J.M., Erwin, J.M., Hof, P.R.: Evolution of specialized pyramidal neurons in primate visual and motor cortex. Brain Behav. Evol. **61**, 28–44 (2003)
4. Braak, H., Braak, E.: Pyramidal cells of Betz within cingulate and precentral gigantopyramidal field in human-brain - Golgi and pigment architectonic study. Cell Tissue Res. **172**, 103–119 (1976)
5. Amunts, K., Schmidt-Passos, F., Schleicher, A., Zilles, K.: Postnatal development of interhemispheric asymmetry in the cytoarchitecture of human area 4. Anat. Embryol. (Berl.) **196**, 393–402 (1997)
6. Pakkenberg, B., Pelvig, D., Marner, L., Bundgaard, M.J., Gundersen, H.J., Nyengaard, J.R., Regeur, L.: Aging and the human neocortex. Exp. Gerontol. **38**, 95–99 (2003)
7. DeFelipe, J., Marco, P., Busturia, I., Merchan-Perez, A.: Estimation of the number of synapses in the cerebral cortex: methodological considerations. Cereb. Cortex **9**, 722–732 (1999)
8. Schleicher, A., Palomero-Gallagher, N., Morosan, P., Eickhoff, S., Kowalski, T., de Vos, K., Amunts, K., Zilles, K.: Quantitative architectonic analysis: a new approach to cortical mapping. Anat. Embryol. (Berl.) **210**, 373–386 (2005)

9. Eickhoff, S.B., Paus, T., Caspers, S., Grosbas, M.H., Evans, A.C., Zilles, K., Amunts, K.: Assignment of functional activations to probabilistic cytoarchitectonic areas revisited. Neuroimage **36**, 511–521 (2007)
10. Eickhoff, S., Stephan, K.E., Mohlberg, H., Grefkes, C., Fink, G.R., Amunts, K., Zilles, K.: A new SPM toolbox for combining probabilistic cytoarchitectonic maps and functional imaging data. Neuroimage **25**, 1325–1335 (2005)
11. Eickhoff, S.B., Heim, S., Zilles, K., Amunts, K.: Testing anatomically specified hypotheses in functional imaging using cytoarchitectonic maps. Neuroimage **32**, 570–582 (2006)
12. Amunts, K., Weiss, P.H., Mohlberg, H., Pieperhoff, P., Gurd, J., Shah, J.N., Marshall, C.J., Fink, G.R., Zilles, K.: Analysis of the neural mechanisms underlying verbal fluency in cytoarchitectonically defined stereotaxic space - the role of Brodmann,s areas 44 and 45. Neuroimage **22**, 42–56 (2004)
13. Makuuchi, M., Grodzinsky, Y., Amunts, K., Santi, A., Friederici, A.D.: Processing non-canonical sentences in Broca's region: reflections of movement distance and type. Cereb. Cortex **23**(3), 694–702 (2013)
14. Grothe, M., Zaborszky, L., Atienza, M., Gil-Neciga, E., Rodriguez-Romero, R., Teipel, S.J., Amunts, K., Suarez-Gonzalez, A., Cantero, J.L.: Reduction of basal forebrain cholinergic system parallels cognitive impairment in patients at high-risk of developing Alzheimer's Disease. Cereb. Cortex **20**, 1685–1695 (2010)
15. Clos, M., Amunts, K., Laird, A., Fox, P.T., Eickhoff, S.B.: Tackling the multifunctional nature of Broca's region meta-analytically: connectivity-based parcellation of area 44. Neuroimage **83**, 174–188 (2013)
16. Caspers, S., Eickhoff, S.B., Zilles, K., Amunts, K.: Microstructural grey matter parcellation and its relevance for connectome analyses. Neuroimage **80**, 18–26 (2013)
17. Herculano-Houzel, S.: The remarkable, yet not extraordinary, human brain as a scaled-up primate brain and its associated cost. Proc. Natl. Acad. Sci. U.S.A. **109**(Suppl 1), 10661–10668 (2012)
18. Hilgetag, C., Barbas, H.: Are there ten times more glia than neurons in the brain? Brain Struct. Funct. **213**, 365–366 (2009)
19. Blinkov, S.M., Glezer, I.I.: The Human Brain in Figures and Tables: A Quantitative Handbook. Basic Books, New York (1986)
20. Amunts, K., Lepage, C., Borgeat, L., Mohlberg, H., Dickscheid, T., Rousseau, M.E., Bludau, S., Bazin, P.L., Lewis, L.B., Oros-Peusquens, A.M., Shah, N.J., Lippert, T., Zilles, K., Evans, A.C.: BigBrain: an ultrahigh-resolution 3D human brain model. Science **340**, 1472–1475 (2013)
21. Amunts, K., Hawrylycz, M., Van Essen, D., Van Horn, J.D., Harel, N., Poline, J.B., De Martino, F., Bjaalie, J.G., Dehaene-Lambertz, G., Dehaene, S., Valdes-Sosa, P., Thirion, B., Zilles, K., Hill, S.L., Abrams, M.B., Tass, P.A., Vanduffel, W., Evans, A.C., Eickhoff, S. B.: Interoperable atlases of the human brain. Neuroimage (2014, in press)
22. Clarke, S.: Callosal connections and functional subdivision of the human occipital lobe. In: Gulyas, B., Ottoson, D., Roland, P.E. (eds.) Functional organization of the human visual cortex, pp. 137–149. Pergamon Press, Oxford (1993)
23. Rockland, K.S.: Visual cortical organization at the single axon level: a beginning. Neurosci. Res. **42**, 155–166 (2002)
24. Le Bihan, D., Mangin, J.F., Poupon, C., Clark, C.A., Pappata, S., Molko, N., Chabriat, H.: Diffusion tensor imaging: concepts and applications. J. Magn. Reson. Imaging **13**, 534–546 (2001)
25. Pierpaoli, C., Jezzard, P., Basser, P.J., Barnett, A., Di Chiro, G.: Diffusion tensor MR imaging of the human brain. Radiology **201**, 637–648 (1996)

26. Wedeen, V.J., Rosene, D.L., Wang, R., Dai, G., Mortazavi, F., Hagmann, P., Kaas, J.H., Tseng, W.Y.I.: The geometric structure of the brain fiber pathways: a continous orthogonal grid. Science **335**, 1628–1634 (2012)
27. Basser, P.J., Jones, D.K.: Diffusion-tensor MRI: theory, experimental design and data analysis - a technical review. NMR Biomed. **15**, 456–467 (2002)
28. Mori, S., van Zijl, P.C.: Fibre tracking: principles and strategies - a technical review. NMR Biomed. **15**, 468–480 (2002)
29. Johansen-Berg, H., Rushworth, M.F.: Using diffusion imaging to study human connectional anatomy. Annu. Rev. Neurosci. **32**, 75–94 (2009)
30. Fornito, A., Bullmore, E.T.: Connectomics: a new paradigm for understanding brain disease. Eur. Neuropsychopharmacol. (2014, in press)
31. Jbabdi, S., Behrens, T.E.: Long-range connectomics. Ann. N. Y. Acad. Sci. **1305**, 83–93 (2013)
32. Van Essen, D.C.: Cartography and connectomes. Neuron **80**, 775–790 (2013)
33. Grefkes, C., Fink, G.R.: Connectivity-based approaches in stroke and recovery of function. Lancet Neurol. **13**, 206–216 (2014)
34. Wang, H., Black, A.J., Zhu, J., Stigen, T.W., Al-Qaisi, M.K., Netoff, T.I., Abosch, A., Akkin, T.: Reconstructing micrometer-scale fiber pathways in the brain: multi-contrast optical coherence tomography based tractography. Neuroimage **58**, 984–992 (2011)
35. de Boer, J.F., Milner, T.E., van Gemert, M.J., Nelson, J.S.: Two-dimensional birefringence imaging in biological tissue by polarization-sensitive optical coherence tomography. Opt. Lett. **22**, 934–936 (1997)
36. Petrides, M., Pandya, D.N.: Distinct parietal and temporal pathways to the homologues of Broca's area in the monkey. PLoS Biol. **7**(8), e1000170 (2009). Epub, 11 Aug 2009
37. Schmahmann, J.D., Pandya, D.N.: Fiber Pathways of the Brain. Oxford University Press, New York (2006)
38. Galuske, R.A., Schlote, W., Bratzke, H., Singer, W.: Interhemispheric asymmetries of the modular structure in human temoral cortex. Science **289**, 1946–1949 (2000)
39. Axer, M., Grässel, D., Kleiner, M., Dammers, J., Dickscheid, T., Reckfort, J., Hütz, T., Eiben, B., Pietrzyk, U., Zilles, K., Amunts, K.: High-resolution fiber tract reconstruction in the human brain by means of three-dimensional polarized light imaging. Front. Neuroinform. **5**, 1–13 (2011)
40. Axer, M., Amunts, K., Gräßel, D., Palm, C., Dammers, J., Axer, H., Pietrzyk, U., Zilles, K.: A novel approach to the human connectome: Ultra-high resolution mapping of fiber tracts in the brain. Neuroimage **54**, 1091–1101 (2011)
41. Vidal, B.C., Mello, M.L.S., Caseiro-Filho, A.C., Godo, C.: Anisotropic properties of the myelin sheath. Acta Histochem. **66**, 32–39 (1980)
42. Jones, C.J.: A new calculus for the treatment of optical systems. J. Opt. Soc. Am. **31**, 488–493 (1941)
43. Breuer, L., Axer, M., Dammers, J.: A new constrained ICA approach for optimal signal decomposition in polarized light imaging. J. Neurosci. Methods **220**, 30–38 (2013)
44. Palm, C., Axer, M., Gräßel, D., Dammers, J., Lindemeyer, J., Zilles, K., Pietrzyk, U., Amunts, K.: Toward ultra-high resolution fiber tract mapping of the human brain - registration of polairization light images and reorientation of fiber vectors. Front. Hum. Neurosci. **4**, 1–16 (2010)
45. Sitt, J.D., King, J.R., Naccache, L., Dehaene, S.: Ripples of consciousness. TINS **17**, 552–554 (2013)

46. http://www.fz-juelich.de/ias/jsc/EN/Expertise/Supercomputers/JUROPA/JUROPA_node.html
47. http://unicore.eu
48. http://uftp-multicast.sourceforge.net/
49. http://nifti.nimh.nih.gov/
50. http://www.hdfgroup.org/HDF5/